JOURNAL OF GUIDANCE, CONTROL, AND DYNAMICS
Vol. 28, No. 4, July–August 2005

Derivation of Formation-Flight Guidance Laws for Unmanned Air Vehicles

Shay Segal,* Joseph Z. Ben-Asher,† and Haim Weiss‡
Technion—Israel Institute of Technology, 32000 Haifa, Israel

A guidance-based approach to formation flight of unmanned air vehicles is presented. Most of the works related to formation flight deal with the control of the relative positions between the vehicles in the formation. In the proposed approach a pursuit law replaces the control law. A new rule of pursuit denoted as detective deviated pursuit is then developed based on known guidance rules. The proposed guidance law regulates the distances between vehicles and the heading angles with respect to the lines of sight. We show that the detective deviated pursuit rule can be applied to formation flight, where the formation geometry determines the guidance-law parameters. The work discusses the conditions for a stable formation flight in the case of a maneuvering leader and proposes a control scheme for implementation. The performance of the new guidance-based formation flight is evaluated via simulations.

Nomenclature

C_D	=	drag coefficient
C_L	=	lift coefficient
D	=	drag
g	=	acceleration caused by gravity
K	=	drag polar constant
K_{xI}	=	integral controller for the x state
K_{xP}	=	proportional controller for the x state
n	=	load factor
R	=	radius
r	=	leader–follower range
T	=	thrust
t	=	time
V	=	velocity
W	=	weight
$\boldsymbol{X}$	=	states vector
x, y	=	inertial coordinates
Γ	=	nondimensional parameter
γ	=	path angle
δ	=	deviation angle
ϵ	=	angle between the line-of-sight (LOS) $F_1 - L$ and LOS $F_2 - F_1$
η	=	throttle position
θ	=	angle between the LOS $F_1 - L$ and the leader's velocity
λ	=	line-of-sight angle
μ	=	bank angle
μ_1, μ_2	=	eigenvalues
χ	=	path angles in the control scheme
ω	=	angular velocity

Subscripts

c	=	command
e	=	error
F	=	follower
L	=	leader
N	=	number of followers in the formation

Received 4 January 2004; revision received 9 May 2004; accepted for publication 28 May 2004. Copyright © 2004 by the American Institute of Aeronautics and Astronautics, Inc. All rights reserved. Copies of this paper may be made for personal or internal use, on condition that the copier pay the $10.00 per-copy fee to the Copyright Clearance Center, Inc., 222 Rosewood Drive, Danvers, MA 01923; include the code 0731-5090/05 $10.00 in correspondence with the CCC.

*Graduate Student, Faculty of Aerospace Engineering; shai@aerodyne.technion.ac.il.

†Associate Professor, Faculty of Aerospace Engineering; yossi@aerodyne.technion.ac.il. Associate Fellow AIAA.

‡Adjunct Senior Teaching Fellow and Lady Davis Visiting Scientist, Faculty of Aerospace Engineering; currently Research Fellow, RAFAEL, Armament Development Authority, Ltd., P.O. Box 2250, Dept. 35, Haifa, Israel; haimw@rafael.co.il.

I. Introduction

UNMANNED air vehicles (UAVs) are becoming an integral part of future military forces and will be used for complex tasks such as reconnaissance, surveillance, close air support, suppression of enemy air defense, aerial refueling, and precision strike missions. To successfully complete such tasks without human intervention and in the presence of large external disturbances, different threats, flight critical failures, and battle damage, there is a growing interest in developing highly efficient autonomous intelligent flight control systems for multiple UAVs.

An effective mission accomplishment with multiple vehicles requires tight guidance and control of individual UAVs flight in a formation. For this reason the problem of formation-flight control of UAVs is currently of wide interest, and a large amount of work has been done on the subject.[1–8] Most of the works related to formation flight deal with the control of the relative positions and consist of variations in the traditional leader/follower formation.[1–4] A leader is chosen to direct the formation, and all other airplanes are expected to maintain a fixed relative distance to the leading airplane. These works discuss the design of an autopilot for the follower, which controls its relative position. Different control approaches have been applied to solve the problem.

The present paper proposes a new guidance-based approach to formation flight of UAVs. The inspiration to this work was taken from the ant-pursuit problem analysis of Ref. 9, which indicates that a simple interaction of players can solve the problem of finding the optimal path between the source and the destination and proves that a global behavior can result from simple and local pursuit rules.

Similar to the ant-pursuit problem, we assume that all of the measurements performed by a vehicle in the formation are relative only to the one in front of it (necessary for collision avoidance). In such a way the measurement problem is simplified (for example, we do not need additional measurements of the formation leader). Moreover, we believe that it mimics the way that birds actually create formation flights.

To present the advantages of the proposed approach, we will use the definition of guidance as a three-level process as described in Ref. 10. According to Ref. 10, guidance is defined as a hierarchical process, which can be said to consist of three levels: geometrical rules, guidance law, and control. The level of this paper is the first level, concentrating on the geometrical rules that lead to formation flights. The treatment of the formation-flight problem by the

guidance-based approach is natural. In our case the target is the formation leader (marked L), and the guided object is the follower (F). The principal difference between a classical guidance problem and the formation-flight problem is that the follower should maintain a constant range from the leader rather than actually intercepting it. In this paper a new rule of pursuit is developed to achieve this purpose. This new guidance law is derived from two known guidance rules: the detective and the deviated pursuit.[10] The new guidance law will be denoted as detective deviated pursuit (DDP).

The advantages of using the guidance approach in the treatment of the formation-flight problem rather than the conventional relative position control approaches lies mainly in the first level of the process: the geometrical rule. This level in the solution of the formation-flight problem yields a complete and deeper understanding of the kinematics of the aircraft taking part in the formation. It produces more general conclusions regarding the maneuvering limits of the formation, the conditions for its stability, etc., that enable obtaining general models for formation flight with a large number of participants. Moreover, because the guidance law (i.e., the second level) is designed to implement the geometrical rule, the velocity commands received by the follower autopilot have a clear physical meaning (usually not the case under the aforementioned direct control approaches). The velocity vector command results directly from the physics of the problem. The analysis is nonlinear, and it retains the physical meaning and has less room for mistakes.

The paper is organized as follows: Sec. II presents the guidance-based approach for the formation control problem and discusses the DDP for N followers in formation. Section III deals with the stability analysis of the proposed guidance law. In Sec. IV we propose a control configuration in which each follower measures its position relative to the preceding one. The simulation results for a formation flight of five F-16 fighters are presented in Sec. V. Finally, conclusions are given in Sec. VI.

II. Formation-Flight Control: A Guidance-Based Approach

A. Detective Deviated Pursuit

The guidance law used for the formation control is based on DDP. Figure 1 describes the basic geometry associated with the DDP approach. It shows a two-vehicle formation consisting of a leader (L) and a follower (F). V_L and V_F are linear velocities, and γ_L and γ_F are the corresponding path angles. Using the notation presented in Fig. 1, the following conditions define a DDP:

1) The follower (F) keeps the range r constant by controlling its own speed (detective condition).

2) The follower's velocity V_F leads the line of sight (LOS) by a constant angle δ (deviation condition).

We limit θ to be $-\pi/2 < \theta < \pi/2$. The imposed limits guarantee that the leader's velocity has no components along the LOS vector in the direction of the follower.

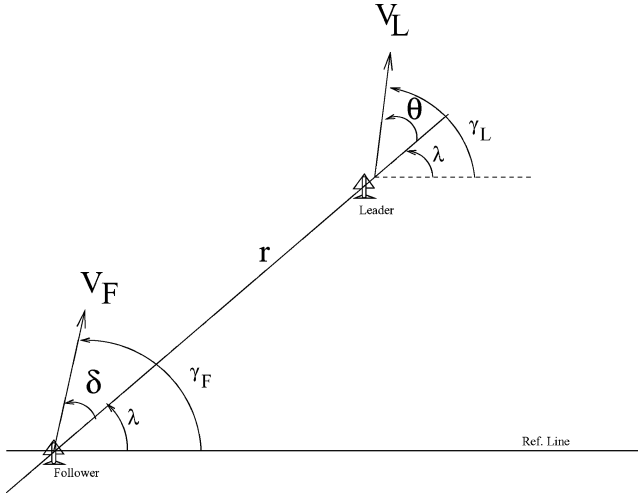

Fig. 1 DDP basic geometry.

Note the following:

1) If the leader moves on a straight line, then γ_L = constant and $\dot{\gamma}_L = 0$.

2) If the leader follows a circle of radius R at constant speed, then $\dot{\gamma}_L = \omega = V_L/R =$ constant.

In this discussion we will always assume $\dot{\gamma}_L \geq 0$; the discussion for negative $\dot{\gamma}_L$ is identical. The constant range requirement leads to the condition

$$\dot{r} = 0 \tag{1}$$

which is equivalent to

$$V_L \cos\theta - V_F \cos\delta = 0 \tag{2}$$

hence $-\pi/2 < \delta < \pi/2$.

The LOS angular rate $\dot{\lambda}$ is calculated by

$$\dot{\lambda} = (1/r)(V_L \sin\theta - V_F \sin\delta) \tag{3}$$

Using Eq. (2), Eq. (3) can be rewritten as

$$\dot{\lambda} = (V_L/r)(\sin\theta - \cos\theta \tan\delta) \tag{4}$$

From the geometry of Fig. 1, the leader's path angle γ_L satisfies

$$\gamma_L = \theta + \lambda \tag{5}$$

Equations (4) and (5) lead to the DDP differential equation

$$\dot{\theta} + (V_L/r)(\sin\theta - \cos\theta \tan\delta) - \dot{\gamma}_L = 0 \tag{6}$$

The solution θ of Eq. (6) is used to calculate the follower path angle γ_F:

$$\gamma_F = \delta + \lambda = \delta + \gamma_L - \theta \tag{7}$$

Remarks:

1) $\dot{\gamma}_L = 0$ (straight path) implies that $\theta = \delta$.

2) $\dot{\gamma}_L = \omega =$ const (circular path) implies that

$$\dot{\theta} + (V_L/r)\sin\theta - (V_L/r)\tan\delta\cos\theta - \omega = 0 \tag{8}$$

Equation (8) can be rewritten in terms of the nondimensional parameter Γ defined by

$$\Gamma = r\omega/V_L = r/R \tag{9}$$

where R is the radius of the circular path performed by the leader.

$$\dot{\theta} = (V_L/r)[(1/\cos\delta)\sin(\delta - \theta) + \Gamma] \tag{10}$$

The solution of Eq. (10) is

$$\theta(t) = 2\arctan\left\{\frac{1}{\Gamma - \tan\delta} + \frac{k_1}{\Gamma - \tan\delta}\cdot\frac{1 + c_1\exp[(k_1 V_L/r)t]}{1 - c_1\exp[(k_1 V_L/r)t]}\right\} \tag{11}$$

if

$$\Gamma^2 < 1 + (\tan\delta)^2 \tag{12}$$

$$\theta(t) = 2\arctan\left\{\frac{k_2\tan[k_1(V_L/r)t + c_2] + 1}{\Gamma - \tan\delta}\right\} \tag{13}$$

if

$$\Gamma^2 > 1 + (\tan\delta)^2 \tag{14}$$

where

$$k_1 = \sqrt{1 + (\tan\delta)^2 - \Gamma^2} \tag{15}$$

$$k_2 = \sqrt{\Gamma^2 - 1 - (\tan\delta)^2} \tag{16}$$

$$c_1 = \frac{-1 - k_1 + (\Gamma - \tan\delta)\tan(\theta_0/2)}{-1 + k_1 + (\Gamma - \tan\delta)\tan(\theta_0/2)} \tag{17}$$

$$c_2 = \arctan\left[\frac{-1 + (\Gamma - \tan\delta)\tan(\theta_0/2)}{k_2}\right] \tag{18}$$

and $\theta(t_0) = \theta_0$. The solution defined by Eq. (11) converges to $2\arctan[(1-k_1)/(\Gamma - \tan\delta)]$ as $t \to \infty$. This value is independent of the initial condition θ_0. The solution defined by Eq. (13) is periodic. We are interested in the solution given by Eq. (11). Note that condition (12) is automatically satisfied if $\Gamma \le 1$ (i.e., the leader's turn radius is greater than or equal to the formation spacing). However for any Γ there is δ for which the condition is satisfied.

B. *N* Follower Formation Flight

Figure 2 describes the geometry associated with one leader and two followers (F_1 and F_2). Applying the DDP approach, we note that follower 1 pursues the leader and follower 2 pursues follower 1. Following the described geometry, we find that

$$\dot{r}_1 = V_L\cos\theta - V_{F_1}\cos\delta_1 \tag{19}$$

$$\dot{r}_2 = V_{F_1}\cos(\delta_1 - \epsilon) - V_{F_2}\cos\delta_2 \tag{20}$$

$$\dot{\lambda}_1 = (1/r_1)\big(V_L\sin\theta - V_{F_1}\sin\delta_1\big) \tag{21}$$

$$\dot{\lambda}_2 = (1/r_2)\big[V_{F_1}\sin(\delta_1 - \epsilon) - V_{F_2}\sin\delta_2\big] \tag{22}$$

The DDP approach requires that $\dot{r}_1 = \dot{r}_2 = 0$.

Therefore,

$$V_{F_1} = V_L\frac{\cos\theta}{\cos\delta_1} \tag{23}$$

$$V_{F_2} = V_L\frac{\cos\theta\cos(\delta_1 - \epsilon)}{\cos\delta_1\cos\delta_2} \tag{24}$$

The angle ϵ between the lines $F_1 - L$ and $F_2 - F_1$ can be calculated as

$$\epsilon = \lambda_2 - \lambda_1 \tag{25}$$

Substituting Eqs. (23) and (24) into Eqs. (21) and (22) and assuming $\dot{r}_1 = \dot{r}_2 = 0$ and $r_1 = r_2 = r$, we obtain that

$$\dot{\epsilon} = \frac{V_L}{r}\left[\frac{\cos\theta}{\cos\delta_1\cos\delta_2}\sin(\delta_1 - \delta_2 - \epsilon) - \frac{\sin(\theta - \delta_1)}{\cos\delta_1}\right] \tag{26}$$

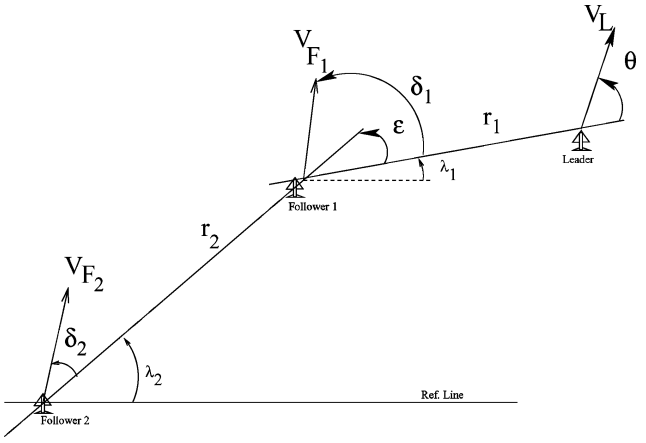

Fig. 2 Three-vehicle formation.

(The case $r_1 \neq r_2$ is not treated here and is left for further research.) The leader path angle γ_L satisfies

$$\gamma_L = \theta + \lambda_1 \tag{27}$$

Using Eqs. (21) and (23), the differential equation for θ can be derived as

$$\dot{\theta} = \frac{V_L}{r}\frac{\sin(\delta_1 - \theta)}{\cos\delta_1} + \dot{\gamma}_L \tag{28}$$

Observe that Eqs. (28) and (26) are partially decoupled. Equation (28) is independent of Eq. (26), whereas Eq. (26) does depend on Eq. (28).

Similarly, we can write the state equations for one leader and N followers. Consider the geometry associated with follower N, follower $N-1$, and follower $N-2$. Based on this geometry, we can write

$$\dot{r}_N = V_{F_{N-1}}\cos(\delta_{N-1} - \epsilon_{N-1}) - V_{F_N}\cos\delta_N \tag{29}$$

$$\dot{\lambda}_N = (1/r_N)\big[V_{F_{N-1}}\sin(\delta_{N-1} - \epsilon_{N-1}) - V_{F_N}\sin\delta_N\big] \tag{30}$$

where

$$V_{F_0} = V_L \tag{31}$$

$$\delta_0 = \theta \tag{32}$$

$$\epsilon_0 = 0 \tag{33}$$

The detective condition is satisfied if $\dot{r}_N = 0$. Hence,

$$V_{F_N} = V_{F_{N-1}}\frac{\cos(\delta_{N-1} - \epsilon_{N-1})}{\cos\delta_N} \tag{34}$$

Substitution of Eq. (34) into Eq. (30) and using $r_N = r$ yields

$$\dot{\lambda}_N = \frac{V_{F_{N-1}}}{r\cos\delta_N}\sin(-\delta_N + \delta_{N-1} - \epsilon_{N-1}) \tag{35}$$

Replacement of N by $N+1$ in Eq. (35) and the use of Eq. (34) leads to

$$\dot{\lambda}_{N+1} = \frac{V_{F_{N-1}}}{r}\frac{\cos(\delta_{N-1} - \epsilon_{N-1})\sin(-\delta_{N+1} + \delta_N - \epsilon_N)}{\cos\delta_N\cos\delta_{N+1}} \tag{36}$$

The angle ϵ_N is defined by

$$\epsilon_N = \lambda_{N+1} - \lambda_N \tag{37}$$

Therefore

$$\dot{\epsilon}_N = \dot{\lambda}_{N+1} - \dot{\lambda}_N$$

$$= \frac{V_{F_{N-1}}}{r}\left[\frac{\cos(\delta_{N-1} - \epsilon_{N-1})\sin(-\delta_{N+1} + \delta_N - \epsilon_N)}{\cos\delta_N\cos\delta_{N+1}}\right.$$

$$\left. - \frac{\sin(-\delta_N + \delta_{N-1} - \epsilon_{N-1})}{\cos\delta_N}\right] \tag{38}$$

Observe that $N = 1$ leads to Eq. (26), where $\epsilon = \epsilon_1$. Recall that $N = 1$ means one leader and one follower.

The preceding derivation can be summarized by the following state-space equations:

$$\dot{\theta} = \frac{V_L}{r}\left[\frac{1}{\cos\delta_1}\sin(\delta_1 - \theta) + \frac{\dot{\gamma}_L r}{V_L}\right]$$

$$\dot{\epsilon}_1 = \frac{V_L}{r}\left[\frac{\cos\theta}{\cos\delta_1\cos\delta_2}\sin(\delta_1 - \delta_2 - \epsilon_1) + \frac{\sin(\theta - \delta_1)}{\cos\delta_1}\right]$$

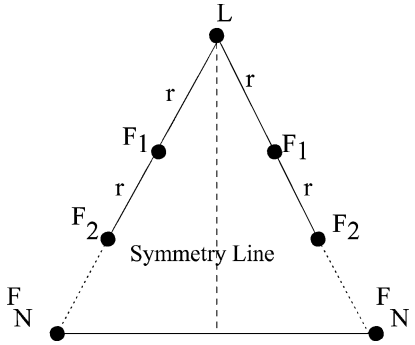

Fig. 3 Arrowhead configuration.

$$\dot{\epsilon}_2 = \frac{V_L}{r}\left[\frac{\cos\theta\cos(\delta_1-\epsilon_1)}{\cos\delta_1\cos\delta_2\cos\delta_3}\sin(\delta_2-\delta_3-\epsilon_2) + \frac{\cos\theta}{\cos\delta_1\cos\delta_2}\sin(\delta_1-\delta_2-\epsilon_1)\right]$$

$$\dot{\epsilon}_3 = \frac{V_L}{r}\left[\frac{\cos\theta\cos(\delta_1-\epsilon_1)\cos(\delta_2-\epsilon_2)}{\cos\delta_1\cos\delta_2\cos\delta_3\cos\delta_4}\sin(\delta_3-\delta_4-\epsilon_3) + \frac{\cos\theta\cos(\delta_1-\epsilon_1)}{\cos\delta_1\cos\delta_2\cos\delta_3}\sin(\delta_2-\delta_3-\epsilon_2)\right]$$

$$\vdots$$

$$\dot{\epsilon}_N = \frac{V_L}{r}\left[\frac{\cos\theta\cos(\delta_1-\epsilon_1)\ldots\cos(\delta_{N-1}-\epsilon_{N-1})}{\cos\delta_1\cos\delta_2\ldots\cos\delta_N\cos\delta_{N+1}}\times\sin(\delta_N-\delta_{N+1}-\epsilon_N) + \frac{\cos\theta\cos(\delta_1-\epsilon_1)\ldots\cos(\delta_{N-2}-\epsilon_{N-2})}{\cos\delta_1\cos\delta_2\ldots\cos\delta_N}\times\sin(\delta_{N-1}-\delta_N-\epsilon_{N-1})\right] \quad (39)$$

Note that a formation of N followers and one leader is described by $N+1$ differential equations, which are one-way coupled. The first state equation is the known DDP equation, which has an analytical solution for a leader in a circular motion with constant angular velocity [Eq. (13)].

C. Conditions for a Flight in a Formation with a Fixed Structure

The popular arrowhead configuration is achieved if the following conditions are satisfied:

1) The state equation (39) has a stable equilibrium point, which satisfies

$$-\pi/2 < \theta^*(\delta_1,\Gamma) < \pi/2 \quad (40)$$

$$\epsilon_i^* = \epsilon_i^*(\delta_1,\ldots,\delta_{i+1},\Gamma) = 0, \qquad i = 1,\ldots,N \quad (41)$$

2) The followers, in the steady state, are structured in two lines as depicted in Fig. 3. The geometry of the right line is a mirror image of the left line.

Other configurations, different from the arrowhead configuration, can be achieved when $\epsilon_i^*(\delta_1,\ldots,\delta_N,\Gamma)\neq 0$. In such cases the lead angles $\delta_i, i=1,\ldots,N$ are used to determine the breaking angles $\epsilon_i^*; i=1,\ldots,N$.

III. Stability Analysis

We show in this section that when the state equations describing the formation of N followers reaches a real equilibrium point it will be a stable one. This is shown by linearization of the state equations about the equilibrium point and by checking the sign of the eigenvalues of the Jacobian matrix. If all eigenvalues of the Jacobian matrix are negative, then the equilibrium point is locally asymptotically stable. First we find the condition for the existence of a real equilibrium point. Then we find the condition at which the eigenvalues of the linearized system are negative. Finally we show that these two conditions are identical, and therefore if there is a real equilibrium point it must be stable. Moreover, by restricting the analysis to the cases of a single and two followers, we show that the condition for a real stable equilibrium point has a clear geometrical meaning.

A. Condition for the Existence of a Real Equilibrium Point

A formation of N followers and one leader is described by $N+1$ differential equation (39). The equilibrium point of the system is obtained when $\dot{\theta}=0$ and $\dot{\epsilon}_i=0$ for $i=1,\ldots,N$. We get

$$\theta^* = \arcsin[\Gamma\cos\delta_1] + \delta_1 \quad (42)$$

[equivalent to $\tan\delta_1 = \tan\theta^* - \Gamma/\cos\theta^*$, which is the steady-state solution of Eq. (11)] and

$$\epsilon_i^* = \delta_i - \delta_{i+1} + \arcsin\left[\frac{\cos\delta_{i+1}}{\cos\left(\delta_{i-1}-\epsilon_{i-1}^*\right)}\sin\left(\delta_{i-1}-\delta_i-\epsilon_{i-1}^*\right)\right] \quad (43)$$

Note that ϵ_i^* is a function of ϵ_{i-1}^*. Thus we can write

$$\epsilon_i^* = \delta_i - \delta_{i+1} + \arcsin\left[\frac{\cos\delta_{i+1}}{\cos(\delta_{i-1}-\epsilon_{i-1})}\sin\left(\delta_{i-1}-\delta_i-\epsilon_{i-1}^*\right)\right]$$

$$\epsilon_{i-1}^* = \delta_{i-1} - \delta_i + \arcsin\left[\frac{\cos\delta_i}{\cos(\delta_{i-2}-\epsilon_{i-2})}\sin\left(\delta_{i-2}-\delta_{i-1}-\epsilon_{i-2}^*\right)\right]$$

$$\epsilon_{i-2}^* = \delta_{i-2} - \delta_{i-1} + \arcsin\left[\frac{\cos\delta_{i-1}}{\cos(\delta_{i-3}-\epsilon_{i-3})}\sin\left(\delta_{i-3}-\delta_{i-2}-\epsilon_{i-3}^*\right)\right]$$

$$\vdots$$

$$\epsilon_1^* = \delta_1 - \delta_2 + \arcsin\left[\frac{\cos\delta_2}{\cos\theta^*}\sin\left(\delta_1-\theta^*\right)\right]$$

$$\theta^* = \arcsin[\Gamma\cos\delta_1] + \delta_1 \quad (44)$$

A recursive substitution leads to

$$\epsilon_i^* = \delta_i - \delta_{i+1} + \arcsin\left[\frac{\cos\delta_1\cos\delta_2,\ldots,\cos\delta_i\cos\delta_{i+1}}{\cos\theta^*,\ldots,\cos\left(\delta_{i-1}-\epsilon_{i-1}^*\right)}\Gamma\right] \quad (45)$$

Hence, by satisfying the inequality

$$-1 \le \left[\frac{\cos\delta_1\cos\delta_2,\ldots,\cos\delta_i\cos\delta_{i+1}}{\cos\theta^*,\ldots,\cos\left(\delta_{i-1}-\epsilon_{i-1}^*\right)}\Gamma\right] \le 1 \quad (46)$$

we get

$$\Gamma \le \left|\frac{\cos\theta^*,\ldots,\cos\left(\delta_{i-1}-\epsilon_{i-1}^*\right)}{\cos\delta_1\cos\delta_2,\ldots,\cos\delta_i\cos\delta_{i+1}}\right| \quad (47)$$

B. Condition for Negative Eigenvalues

From Eq. (39) we obtain an upper triangular Jacobian matrix for the linearized system:

$$\begin{bmatrix} \frac{\partial\dot{\theta}}{\partial\theta} & 0 & 0 & 0 & \dots, & 0 \\ \frac{\partial\dot{\epsilon}_1}{\partial\theta} & \frac{\partial\dot{\epsilon}_1}{\partial\epsilon_1} & 0 & 0 & \dots, & 0 \\ \frac{\partial\dot{\epsilon}_2}{\partial\theta} & \frac{\partial\dot{\epsilon}_2}{\partial\epsilon_1} & \frac{\partial\dot{\epsilon}_2}{\partial\epsilon_2} & 0 & \dots, & 0 \\ \vdots & & & & & \\ \frac{\partial\dot{\epsilon}_N}{\partial\theta} & \dots, & \dots, & \dots, & \dots, & \frac{\partial\dot{\epsilon}_N}{\partial\epsilon_N} \end{bmatrix}\Bigg|_{\epsilon_i=\epsilon_i^*,\ i=1,\dots,N,\theta=\theta^*} \tag{48}$$

Therefore the eigenvalues are the values on the diagonal. For (at least) marginal stability we require

$$\left.\frac{\partial\dot{\epsilon}_i}{\partial\epsilon_i}\right|_{\epsilon_i=\epsilon_i^*,\ i=1,\dots,N} \le 0 \tag{49}$$

Thus,

$$\left.\frac{\partial\dot{\epsilon}_i}{\partial\epsilon_i}\right|_{x=x^*} = -\frac{V_L}{r}\left[\frac{\cos\theta^*\cos\left(\delta_1-\epsilon_1^*\right),\dots,\cos\left(\delta_{i-1}-\epsilon_{i-1}^*\right)}{\cos\delta_1\cos\delta_2,\dots,\cos\delta_i\cos\delta_{i+1}} \times \cos\left(\delta_i-\delta_{i+1}-\epsilon_i^*\right)\right] \le 0, \qquad i=1,\dots,N \tag{50}$$

Because $r, V_L > 0$, the stability condition becomes

$$\left[\frac{\cos\theta^*\cos\left(\delta_1-\epsilon_1^*\right),\dots,\cos\left(\delta_{i-1}-\epsilon_{i-1}^*\right)}{\cos\delta_1\cos\delta_2,\dots,\cos\delta_i\cos\delta_{i+1}}\cos\left(\delta_i-\delta_{i+1}-\epsilon_i^*\right)\right] \ge 0, \qquad i=1,\dots,N \tag{51}$$

C. Real Equilibrium Point Is Stable

Substituting Eq. (45) into Eq. (51), we obtain

$$\frac{\cos\theta^*\cos\left(\delta_1-\epsilon_1^*\right),\dots,\cos\left(\delta_{i-1}-\epsilon_{i-1}^*\right)}{\cos\delta_1\cos\delta_2,\dots,\cos\delta_i\cos\delta_{i+1}}\cos \times\left\{\arcsin\left[\frac{\cos\delta_1\cos\delta_2,\dots,\cos\delta_i\cos\delta_{i+1}}{\cos\theta^*\cos\left(\delta_1-\epsilon_1^*\right),\dots,\cos\left(\delta_{i-1}-\epsilon_{i-1}^*\right)}\Gamma\right]\right\} \ge 0 \tag{52}$$

Define

$$A \equiv \left[\frac{\cos\delta_1\cos\delta_2,\dots,\cos\delta_i\cos\delta_{i+1}}{\cos\theta^*\cos\left(\delta_1-\epsilon_1^*\right),\dots,\cos\left(\delta_{i-1}-\epsilon_{i-1}^*\right)}\right] \tag{53}$$

We get the following stability condition:

$$A^{-1}\cos[\arcsin(A\Gamma)] \ge 0 \tag{54}$$

which is satisfied if and only if $A^{-1} \ge 0$ and $|A\Gamma| \le 1$. Thus,

$$\Gamma \le \left|\frac{\cos\theta^*\cos\left(\delta_1-\epsilon_1^*\right),\dots,\cos\left(\delta_{i-1}-\epsilon_{i-1}^*\right)}{\cos\delta_1\cos\delta_2,\dots,\cos\delta_i\cos\delta_{i+1}}\right| \tag{55}$$

which is the same as Eq. (47).

We need to prove that $A^{-1} \ge 0$. From the detective conditions (23) and (24)

$$\frac{\cos\delta_i}{\cos\left(\delta_{i-1}-\epsilon_i^*\right)} > 0 \tag{56}$$

$$\frac{\cos\theta^*}{\cos\delta_1} > 0 \tag{57}$$

also $\cos(\delta_{i+1}) > 0$; hence, $A^{-1} \ge 0$.

We conclude that if there is an equilibrium point, it must be stable. This is true for formation with any number of participants when the leader is following a straight or a circular path. Notice that Γ is not bounded. For all Γ there are $\delta_i, i=1,\dots,N$ such that Eq. (55) is satisfied.

D. Single-Follower Case

The differential equation associated with this case is the DDP equation (6). The related equilibrium point is obtained when $\dot{\theta}=0$. Equation (6) can be rewritten as

$$\dot{\theta} = (V_L/r)\left\{[1+(\tan\delta)^2]^{\frac{1}{2}}\sin(\delta-\theta)+\Gamma\right\} \tag{58}$$

where

$$\Gamma = r\dot{\gamma}_L/V_L \tag{59}$$

The equilibrium point of Eq. (58) is (notice that $|\delta|<\pi/2$ and $|\delta|<\pi/2$)

$$\theta^* = \arcsin\left\{\Gamma\Big/[1+(\tan\delta)^2]^{\frac{1}{2}}\right\}+\delta \tag{60}$$

We can see that the equilibrium point is a function of δ and Γ. The following condition guarantees a real equilibrium point:

$$\Gamma \le [1+(\tan\delta)^2]^{\frac{1}{2}} \tag{61}$$

Linearizing Eq. (58) around θ^* entails

$$\dot{\theta} \simeq -(V_L/r)\left\{[1+(\tan\delta)^2]^{\frac{1}{2}}\cos(\delta-\theta^*)\right\}(\theta-\theta^*) \tag{62}$$

From Eq. (60) we get that $\cos(\delta-\theta^*) \ge 0$; hence,

$$-(V_L/r)\left\{[1+(\tan\delta)^2]^{\frac{1}{2}}\cos(\delta-\theta^*)\right\} \le 0 \tag{63}$$

Thus any real equilibrium is also (at least marginally) stable.

Remarks:

1) If $\Gamma \le 1$, then $\Gamma \le [1+(\tan\delta)^2]^{\frac{1}{2}}$ for all δ, and Eq. (58) has a real stable equilibrium point. Note that the same result has been obtained by the analytical solution.

2) If

$$1 < \Gamma \le \left[1+(\tan\delta_{\rm cr})^2\right]^{\frac{1}{2}} \tag{64}$$

where

$$\delta_{\rm cr} = \arctan\left[(\Gamma^2-1)^{\frac{1}{2}}\right] = \pi/2-\arcsin(1/\Gamma) \tag{65}$$

then $|\delta| \ge \delta_{\rm cr}$ guarantees that Eq. (58) has a stable equilibrium point. Figure 4 describes θ^* as a function of δ for different values of Γ. Notice that θ^* is limited for $\Gamma > 1$. (The limit is obtained from $\delta = \delta_{\rm cr}$.)

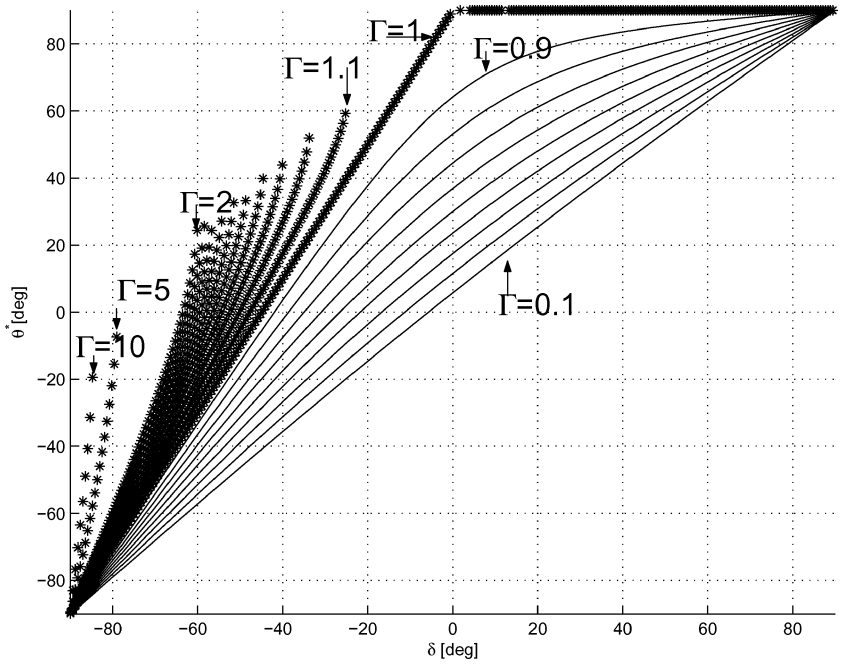

Fig. 4 θ^* vs δ for different values of Γ.

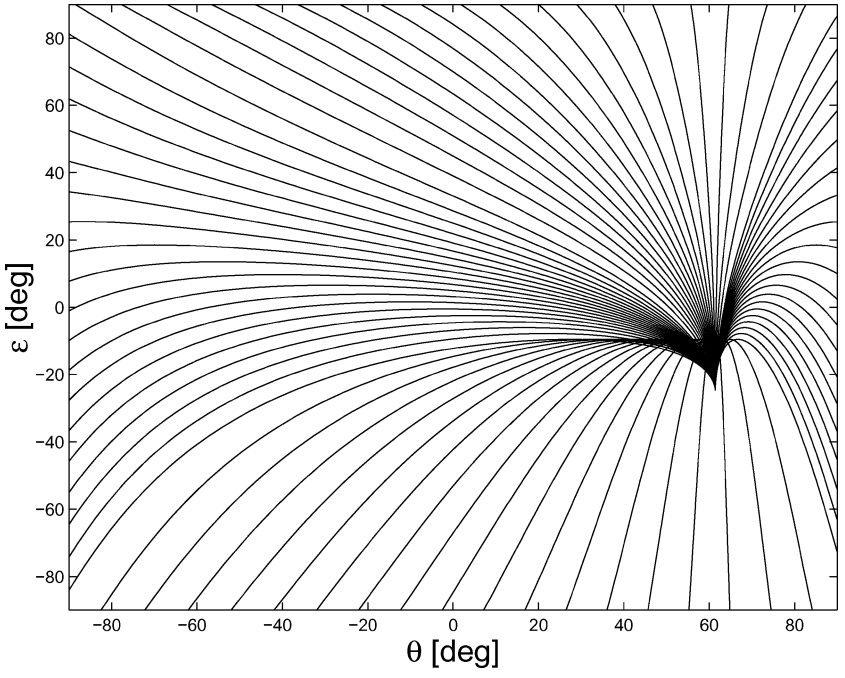

Fig. 5 Typical trajectories in the $\theta - \epsilon$ plane where $\delta_1 = \delta_2 = 45$ deg.

E. Two-Follower Case

In this case the requirement $\dot{\theta} = 0, \dot{\epsilon} = 0$ leads to

$$\theta^* = \arcsin(\Gamma \cos \delta_1) + \delta_1 \tag{66}$$

$$\epsilon^* = \delta_1 - \delta_2 - \arcsin\left[\frac{\Gamma \cos \delta_1 \cos \delta_2}{\cos \theta^*}\right]$$

$$= \delta_1 - \delta_2 - \arcsin\left[\frac{\sin\left(\theta^* - \delta_1\right) \cos \delta_2}{\cos \theta^*}\right] \tag{67}$$

Assuming that $\theta = \theta^*$ is real and therefore stable, we can find the condition for which ϵ^* is real. Following Eq. (67), the satisfaction of the inequality

$$-1 \leq \frac{\sin\left(\theta^* - \delta_1\right) \cos \delta_2}{\cos \theta^*} \leq 1 \tag{68}$$

guarantees that $\epsilon = \epsilon^*$ is a real equilibrium point. As in the preceding case of θ^*, it can be shown that a real equilibrium point $\epsilon = \epsilon^*$ is necessarily stable. The proof is based on linearization of Eqs. (26) and (28) at the vicinity of (θ^*, ϵ^*). The Jacobian calculated at the equilibrium point has two eigenvalues that are nonpositive and real as long as inequality (68) is satisfied:

$$\mu_1 = -\frac{V_L}{r} \frac{\cos\left(\delta_1 - \theta^*\right)}{\cos \delta_1} \tag{69}$$

$$\mu_2 = -\frac{V_L}{r} \frac{\cos \theta^* \cos\left(\delta_1 - \delta_2 - \epsilon^*\right)}{\cos \delta_1 \cos \delta_2} \tag{70}$$

Figure 5 presents typical trajectories in the $\theta - \epsilon$ plane where $\delta_1 = \delta_2 = 45$ deg. The figure shows a stable attraction point.

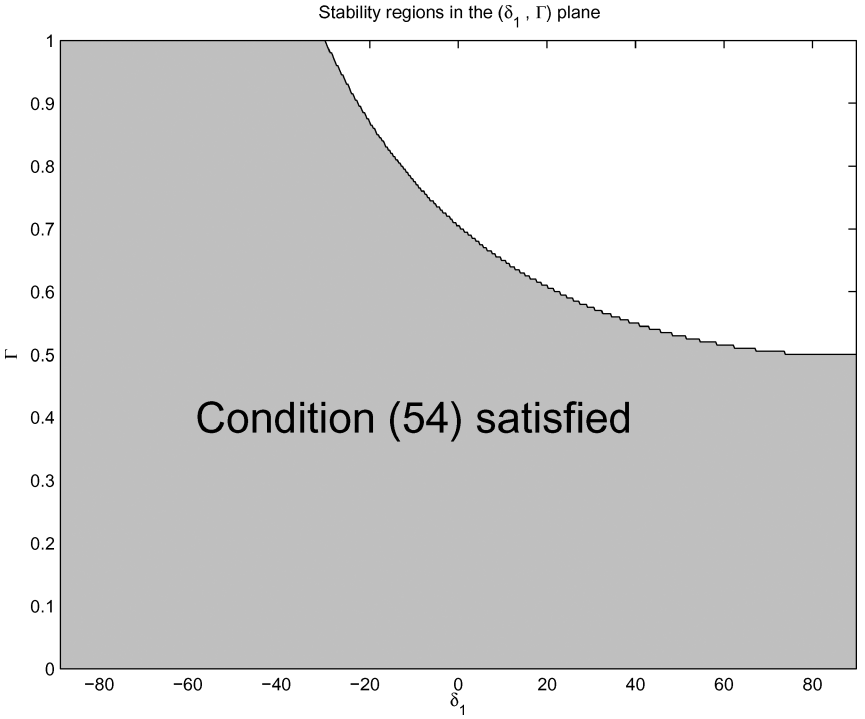

Fig. 6 Local stability region for a leader and two followers.

F. Further Analysis of the Equilibrium-Point Condition

Substituting Eq. (66) into Eq. (68) leads to

$$-\frac{\cos\theta^*}{\cos\delta_1\cos\delta_2} \le \Gamma \le \frac{\cos\theta^*}{\cos\delta_1\cos\delta_2} \tag{71}$$

where δ_1, δ_2, and θ are assumed to be in the range $(-\pi/2, \pi/2)$. Because $\Gamma = r/R \ge 0$, we get the following condition for a real equilibrium point:

$$\Gamma \le \frac{\cos\theta^*}{\cos\delta_1\cos\delta_2} \tag{72}$$

Because $0 \le |\delta_2| \le \pi/2$, then the following relation holds:

$$\frac{\cos\theta^*}{\cos\delta_1} \le \frac{\cos\theta^*}{\cos\delta_1\cos\delta_2} \tag{73}$$

Therefore a stronger condition is

$$\Gamma < \cos\theta^* \Big/ \cos\delta_1 \tag{74}$$

Substitution of Eq. (66) into Eq. (74) leads to

$$\Gamma < \frac{\cos[\arcsin(\Gamma\cos\delta_1) + \delta_1]}{\cos\delta_1} \tag{75}$$

The solution for the inequality (75) is indicated in the painted area of Fig. 6. We can see that for $\Gamma < 0.5$ the inequality (75) is always satisfied (i.e., for all δ). Recall that in a formation flight with one leader and one follower we have found that $\Gamma < 1$ guarantees a real stable equilibrium point (for all δ). We observe now that $\Gamma < \frac{1}{2}$ guarantees a real stable equilibrium point for a formation with one leader and two followers for all δ. This observation leads to the conjecture that for a formation flight consisting of one leader and N followers the condition $\Gamma < 1/N$ will guarantee real stable equilibrium point for all δ.

IV. Formation-Flight Control

The proposed control is based on measurements of position and velocity and uses the guidance law of the preceding sections. For simplicity, we assume that the participants have complete information regarding these measurements with respect to Earth. It can be shown, however, that relative position and velocities, and even LOS angles and relative velocities, are in fact sufficient. Figure 7 depicts the basic control configuration where the states X^L, X^F contain the associated inertial coordinates x, y; the speed V; and the path angle χ. The last two are the controlled variables. For given $\delta_1, \ldots, \delta_N$, the measurements x_{FN}, y_{FN}, x_{FN-1}, y_{FN-1} enable the calculation of the LOS angle λ_N:

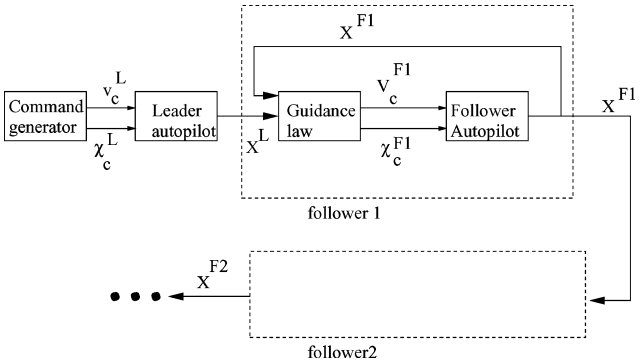

Fig. 7 Proposed control configuration.

$$\lambda_N = \arctan\left[\frac{y_{F_{N-1}} - y_{F_N}}{x_{F_{N-1}} - x_{F_N}}\right] \tag{76}$$

The lead angle of the leader is calculated by

$$\theta = \chi^L - \lambda_1 \tag{77}$$

The guidance commands $\chi_c^{F_N}$, $v_C^{F_N}$ are defined as

$$\chi_c^{F_N} = \delta_N + \lambda_N \tag{78}$$

$$v_C^{F_N} = \frac{\cos(\delta_{N-1} - \epsilon_{N-1})}{\cos\delta_N} v^{F_{N-1}} \tag{79}$$

where

$$\epsilon_{N-1} = \lambda_N - \lambda_{N-1} \tag{80}$$

The autopilot control loops are depicted in Fig. 8 and consist of simple proportional + integral (PI) speed and heading controllers.

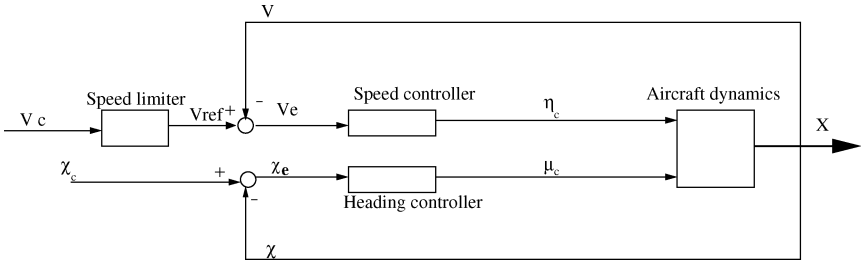

Fig. 8 Autopilot configuration.

(Other schemes can also be used for the same purpose.[11]) Notice that we control $\dot{r}$ and not r under this simplified scheme:

$$\eta_c = K_{V_p} V_e + \left(K_{V_I}/s\right) V_e \tag{81}$$

$$\mu_c = K_{\mu_p} \chi_e + \left(K_{\mu_I}/s\right) \chi_e \tag{82}$$

The speed is limited by the stall velocity V_{stall}. The variables η_c and μ_c denote the throttle position and the bank angle commands, respectively. The value of $\delta_i, i = 1, \ldots, N$ is preselected. The selection of the lead angles $\delta_1, \ldots, \delta_N$ is discussed in Ref. 11.

V. Simulation

A. Modeling

The equation of motion and the aerodynamic forces are derived for a point mass with two degrees of freedom. The simulation uses the following assumptions: 1) planar motion in the horizontal plane at constant altitude; 2) constant weight vehicle; 3) thrust in the velocity direction; 4) two control variables, the bank angle μ and the throttle position η; and 5) decoupled first-order vehicle dynamics for μ and η. The equations of motion are given in an inertial frame and described by

$$\dot{x} = V \cos \chi \tag{83}$$

$$\dot{y} = V \sin \chi \tag{84}$$

$$\dot{V} = (g/W)(T - D) \tag{85}$$

$$\dot{\chi} = (g/V) n \sin \mu \tag{86}$$

where

$$\mu/\mu_c = 1/(1 + s\tau_\mu), \qquad \tau_\mu = 0.2 \text{ s (typical value)} \tag{87}$$

The thrust model was taken from Ref. 12:

$$T_{\max}(h) = T_0 - h(T_0/16{,}764) \tag{88}$$

where

$$T = \eta T_{\max}(h) \tag{89}$$

h is the aircraft altitude, and

$$\eta/\eta_c = 1/(1 + s\tau_\eta), \qquad \tau_\eta = 0.2 \text{ s (typical value)}$$

$$0 \le \eta_c < 1 \tag{90}$$

The aerodynamic model is related to drag only:

$$D = D_0 + n^2 D_i \tag{91}$$

$$D_0 = qSC_{D_0}, \qquad D_i = K(W/qS)^2 \tag{92}$$

where q is the dynamic pressure, S the wing area, and C_{D_0} the zero-lift drag coefficient. The simulation also includes air brakes in order to obtain faster deceleration. The air brake is modeled by a continuous function that is driven by the speed error and generates drag:

$$D_{\text{Air-Brake}} = -K_{\text{air-brake}} V_e \tag{93}$$

The load factor n is bounded by the structural load and satisfies

$$n \le n_{\max} \tag{94}$$

In addition, the load factor is bounded by the maximal lift coefficient $C_{L_{\max}}$ such that

$$n \le n_L = (qS/W) C_{L_{\max}} \tag{95}$$

The bound on the load factor leads to a bound on the bank angle

$$|\mu| \le \arccos(1/n_{\max}) \tag{96}$$

Table 1 F-16 parameters

Parameter	Notation	Value
Wing area	S	27.87
Wing span	b	9.14
Aspect ratio	AR	3
Zero-lift drag coefficient	C_{D_0}	0.015
Drag polar constant	K	0.02
Maximum lift coefficient	$C_{L_{\max}}$	1.5
Structural limit	$n_{\max}$	9 g
Mass	m	11,336.4 kg
Maximum thrust without after burner	$T_{\max}$	6,500 kg
Maximum air-brake drag	$K_{\text{air-brake}}$	3,000 Nt

Table 2 Autopilot parameters

Parameter	Notation and value
Speed controller	$K_{\text{vp}} = 1$, $K_{\text{VI}} = 0.3$
Heading controller	$K_{\mu\text{p}} = 10$, $K_{\mu I} = 10$
Speed limiter	$V_{\text{stall}} = 90$ m/s

Table 1 (Ref. 13) presents the F-16 parameters used in the simulation.

The autopilot parameters are summarized in Table 2.

B. Simulation Results

The simulation demonstrates the formation flight of five F-16 aircraft in an arrowhead configuration. The formation consists of a leader and four followers. F1 and F3 are the first and the second followers from the left, whereas F2 and F4 are the first and second followers from the right. The deviation angles are $\delta_1 = \delta_3 = 45$ deg for the left followers and $\delta_2 = \delta_4 = -45$ deg for right followers. The relative nominal range between the aircraft are selected to be $100\sqrt{2}$ m. In the presented example, the leader performs a straight path followed by a circular path with constant angular velocity, and then it returns to a straight path. Specifically, the leader vehicle's heading command is 0 deg for $0 < t < 90$ s; it then increases at a constant rate of 0.9 deg per second (i.e., $\omega = 0.0157$ rad/s) for $90 < t < 140$ s. Finally it returns to constant heading for $140 < t < 240$ s. The velocity command for the leader is 100 m/s. The leader vehicle's initial heading and velocity are 0 deg and 100 m/s, respectively. All of the followers have the same

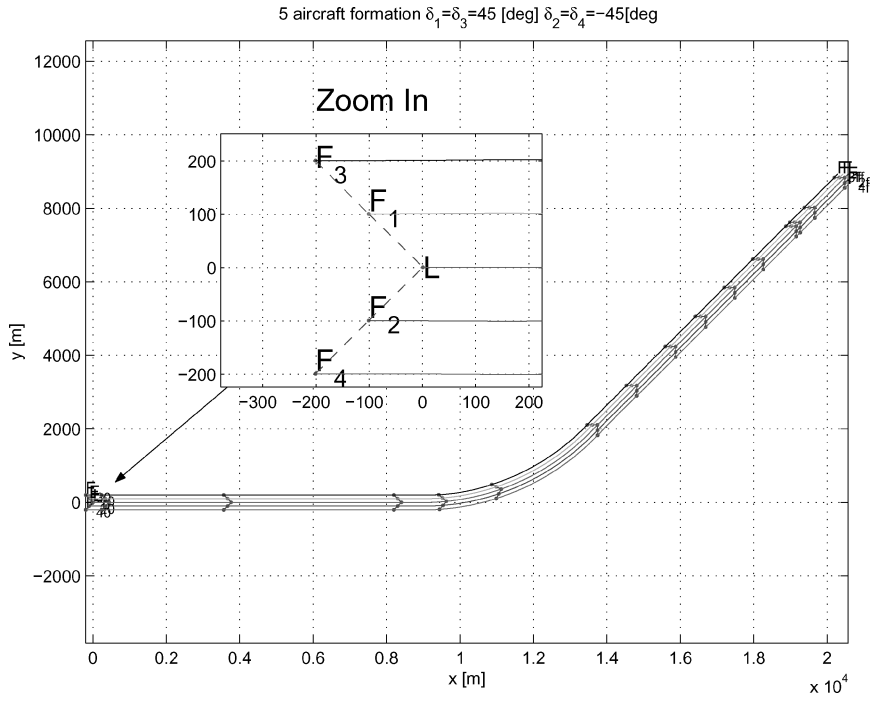

Fig. 9 Trajectories of five F-16 in arrowhead configuration.

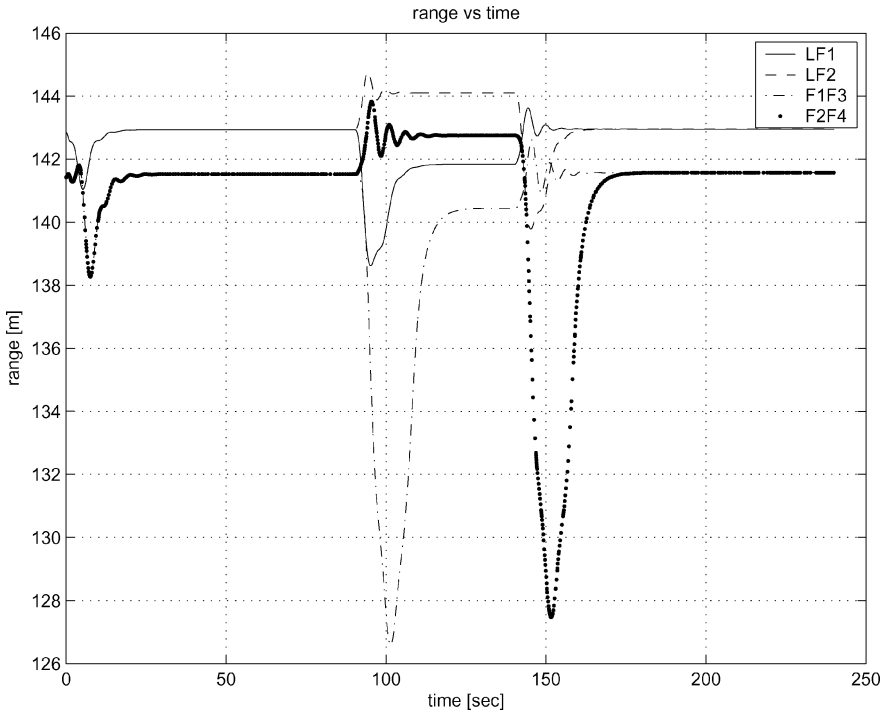

Fig. 10 Range between the aircraft.

initial heading and velocity as the leader. Note that the conditions for stability are satisfied.

Figure 9 presents the aircraft trajectories. As can be seen, the five F-16 aircraft stay in an arrowhead formation during the entire flight even in the face of maneuvering. The relative ranges on the LOS are shown in Fig. 10. Keeping in mind that the desirable range is about 142 m, we make the following observations:

1) Along the straight paths (i.e., $0 < t < 90$ and $140 < t < 240$ s) the relative ranges between all of the aircraft stay close to the initial value. (Recall that in this control scheme r is not directly controlled. Other control loops can use also r to eliminate the small steady-state error.)

2) Flying on a circular path ($90 < t < 140$ s) causes the range to deviate from the desired value in a different manner for the left and right followers: left followers (F1, F3) exhibit maximum deviation at the beginning of the turn, and right followers (F2, F4) exhibit maximum deviation at the end of the turn.

3) The behavior of the error (between the desired and obtained relative ranges) for first followers (F1, F2) and second followers (F3, F4), is similar in nature but for second followers is more drastic.

To understand the reason for these results, we recall that the left followers (F1, F3) are interior to the turn and the right followers (F3, F4) are exterior one. Thus, to keep the formation, the left followers need to decelerate at the beginning of the turn, whereas the right followers need to decelerate at the end of the turn. The behavior of the speed controller suffers from the fact that slowing down is obtained by the uncontrolled drag forces (negative thrust cannot be obtained) and the air brakes. Hence, the throttle limits [Eq. (93)]

and the max air brakes determine the behavior of the loop. When entering the turn, the left followers limited deceleration rate causes the range error. The right followers need to decelerate at the end of the turn in order to return the straight flight; thus, they get the maximal error at the end of the turn.

VI. Conclusions

The paper demonstrates that a formation flight can be achieved by using a simple guidance law, whose parameters are determined by the formation geometry. A guidance law denoted as detective deviated pursuit is developed and implemented for flight formations. Conditions for stability that can always be satisfied with the right choice of deviation angles are formulated. For formation with $r/R \leq 1/N$ (i.e., when the ratio of the formation spacing to the leader's turn radius is less than $1/N$), it was conjectured that the stability conditions are satisfied for all δ. The performance of five F-16 formation is evaluated via two-dimensional simulation, and the results indicate satisfactory performance even under maneuvering conditions. The performance obtained is adequate for a ferry flight of unmanned air vehicles but is not tight enough for the formation during an autonomous aerial refueling and similar tasks.

References

[1]D'Azzo, J. J., Pachter, M., and Dargan, J. L., "Automatic Formation Flight Control," *Journal of Guidance, Control, and Dynamics*, Vol. 17, No. 6, 1994, pp. 1380–1383.

[2]Pachter, M., Proud, A. W., and D'Azzo, J. J., "Close Formation Flight Control," AIAA Paper 99-4207, Aug. 1999.

[3]Chichka, D. F., Wolfe, J. D., and Speyer, J. L., "Decentralized Controllers for Unmanned Aerial Vehicle Formation Flight," AIAA Paper 96-3833, July 1996.

[4]Boskovic, J. D., Li, Sai-Ming, and Mehra, R. K., "Globally Stable Automatic Formation Flight Control In Two Dimensions," AIAA Paper 2001-4046, Aug. 2001.

[5]Pollini, L., Giulietti, F., and Innocenti, M., "Autonomous Formation Flight," *IEEE Control Systems Magazine*, Vol. 20, No. 6, 2000, pp. 34–44.

[6]Pollini, L., Giulietti, F., and Innocenti, M., "Formation Flight Control: A Behavioral Approach," AIAA Paper 2001-4239, Aug. 2001.

[7]Reynolds, C. W., "Flocks, Herds and Schools: A Distributed Behavioral Model," *Computer Graphics*, Vol. 21, No. 4, 1987, pp. 25–34.

[8]Anderson, M. R., and Robbins, A. C., "Formation Flight as a Cooperative Game," AIAA Paper 98-4124, Aug. 1998.

[9]Bruckstein, A. M., "Why the Ant Trails Look So Straight and Nice," *Mathematical Intelligencer*, Vol. 15, No. 2, 1993, pp. 58–62.

[10]Shneydor, N. A., *Missile Guidance and Pursuit*, Horwood Publishing, Chichester, England, U.K., 1998, pp. 1, 2.

[11]Segal, S., "A Derivation of Guidance Laws for UAVs Formation Flight," M.S. Thesis, Faculty of Aerospace Engineering, Technion—Israel Inst. of Technology, Haifa, Israel, Sept. 2003.

[12]Raymer, Daniel P., *Aircraft Design: A Conceptual Approach*, AIAA, Washington, DC, 1989, pp. 1–5.

[13]Hall, James K., "Three Dimensional Formation Flight Control," M.S. Thesis, Air Force Inst. of Technology, Wright–Patterson AFB, OH, March 2000.